공학석사학위논문

# Study on passivation film stability on $LiNi_{0.5}Co_{0.2}Mn_{0.3}O_2$ electrode using linear sweep thermammetry(LSTA)

## LSTA를 이용한 $LiNi_{0.5}Co_{0.2}Mn_{0.3}O_2$의 피막 안정성 연구

2014년 2월

서울대학교 대학원

화학생물공학부

정 유 라

# Study on passivation film stability on $LiNi_{0.5}Co_{0.2}Mn_{0.3}O_2$ electrode using linear sweep thermammetry(LSTA)

## LSTA를 이용한 $LiNi_{0.5}Co_{0.2}Mn_{0.3}O_2$의 피막 안정성 연구

지도교수 오 승 모

이 논문을 공학석사 학위논문으로 제출함

**2014년 02월**

서울대학교 대학원

화학생물공학부

정 유 라

정유라의 공학석사학위 논문을 인준함

**2014년 02월**

위 원 장 _____

부위원장 _____

위 원 _____

# Abstract

Nowadays, application range of lithium ion batteries (LIB) is begin to change from small power devices (e.g. IT devices) to large scale energy storage systems (e.g. electrical vehicle (EV), large scale energy storage systems (ESSs)). From this paradigm change, cycleability of fabricated battery system is more and more important than previous one. And especially, commercialized electrode materials are stable at long-term operation. In this case, passivation film stability is a point to be considered. Therefore, stabilization of this interphase is crucial. In this sense, various additives are currently being studied to stabilize the surface film for enhancing cycleability of battery system. Previously, evaluation sequences of suggested additives are time and cost consuming process. This process included long-term galvanostatic charge/discharge step, AC impedance for resistance measurement and XPS technique for seeing surface characteristics. As we can see the name of analysis technique, these methods are not economically favorable and also time involved cases. However, in industrial aspect, fast with accuracy and economy is needed for testing suggested additives.

In this study, we suggest LSTA(Linear Sweep Thermmametry) technique for

testing surface film characteristics with various additives and diverse temperature. LSTA shows cathodic or anodic currents on working electrode at fixed voltage with temperature sweep. In this case, LSTA is preceded after formation of surface film, therefore, in this experiment, anodic current shown by LSTA with temperature sweep means stability of surface film. From this basis, we predict surface film stability with additive variation at certain temperature. And by using stable electrode material with layered structure, $LiNi_{0.5}Co_{0.2}Mn_{0.3}O_2$ (NCM 523), we can apply this measured relative surface film stability to predict long-term cycleability of various temperatures at certain voltage cut-off cycling with used additives.

In this research, we use non-additive included electrolyte, vinylene carbonate (VC) and propane sultone (PS) 2 *wt*. % added electrolyte solution. In previous reported studies, VC shows unstable feature and PS demonstrates stable characteristic at high temperature and voltage cycling. From selection of these known additives, we can define validation of suggested tool. Also, by choose two temperature cases with room temperature (25 $^0$C) and high temperature (60 $^0$C), temperature dependency of additives are also predicted and confirmed. In room temperature (25 $^0$C) case, three electrolytes show no meaningful difference in anodic current measured by LSTA technique. And this tendency is also found at cycle performance of three electrolyte solution with NCM 523

active material. Furthermore, increment of resistance measured by AC impedance shows same trend with LSTA and cycle data. At high temperature (60 $^{0}$C) condition, three electrolytes show different stability of surface film with PS, non-additive, VC, in sequence. Therefore, we can predict cycleability as that sequence. And in real evaluation of cycle performances of three electrolyte solutions with same active material, NCM 523, demonstrate same tendency as same with we predicted in LSTA data. In nyquist plots of three samples shows resistance difference of three samples with same trends, and also that sequence is also found at film thickness after cycling by XPS spectra.

From these results, we can state that LSTA technique shows stability of surface film generated by additive variation. By using this technique for testing additive validation, time and cost saving at industrial field is expected.

**Keywords**: Lithium secondary batteries, LSTA(Linear sweep thermammetry), passivation film, positive electrode, additives

Student Number: 2012-22586

# List of Figures

# List of Tables

# Contents

# 1. Introduction

Secondary battery systems receive attentions with developing of small IT devices. And with demanding of electricity is even higher than previous centuries, proper use of generated electricity is essential for future society. And one of possible secondary battery system for these applications is lithium ion batteries. Also, according to change of paradigm, cycleability of battery systems is more and more important.

Roughly say, factors determining cycle performance of battery system are intrinsic material properties of negative and positive electrode, separator and electrolyte solution. And also, stability of surface film generated by oxidation or reduction of organic electrolyte is also important feature. Because of restricted electrochemical stability window of used carbonate based electrolyte solution, formation of passivation film is inevitable phenomenon. Therefore, formation of stable surface film on active materials is significant. If stability of passivation film is not enough durable to prevent further electrochemical decomposition of electrolyte, capacity degradation is severe in full cell configuration. This situation is originated with two main factors. One is consuming limited lithium source in positive electrode material with electrolyte

decomposition. The other is increased polarization by previous stated decomposition of electrolyte reaction.

To handling this crucial problem, additives are considered for solution for this. Especially, in this experiment, film forming agent is applied for solving this problem. Typical examples of this type of additives are reduction or oxidation type. Generally, reduction and oxidation type additives have double bonds in their structure. From this feature, added additives are decomposed before decomposition of bulk electrolyte. And if decomposed products have stable electrochemical properties, surface stability and inhibition of gas evolution are improved..

In cell operation, production of generation of additional surface film makes capacity degradation of cell by increased polarization. To minimize this abuse condition, formation of stable surface film is essential. Therefore, selecting the best additive at specified electrochemical characterization of cell is important. However, in previous studies show a lot of time and cost involved analysis and tests. To enhance this characteristic, LSTA is applied as facile tool for testing additives in this study. Oxidation currents in LSTA tool have similar tendency with stability of surface film. Therefore, it is easy to say LSTA shows stability of surface films. From this reason, we can predict cycleability of various additives applied cells by simple method. To verify this tool, propane sultone

(PS), vinylene carbonate (VC) and non-additive cases are applied as evidence. And finally, after those verifications, we suggest LSTA as facile and simple tool for forecasting cycleabilities with variation of electrolytes.

.

# 2. Backgrounds

## 2.1. Characteristics and fundamentals of lithium ion batteries

### 2.1.1. Fundamentals of lithium ion batteries

After commercialized by SONY, lithium ion batteries receive attention as most probable secondary battery system form small power devices to large scale energy storage systems. Lithium ion battery systems uses wide electrochemical electrolyte for enduring working voltage of cell, therefore high energy density of cell is expected. Conventional lithium ion secondary battery system is composed of four essential components, negative and positive electrode, separator for inhibiting physical shortage and carbonate based organic electrolyte solution.

Most used negative electrode material is carbonaceous material, especially graphite. Graphite is well-known with its electrochemical reversibility of lithium ion insertion and de-insertion. In charging of full cell, intercalation of lithium ion in graphite interlayer is preceded and discharging vice versa. And

positive electrode material, for example lithium cobalt oxide, is usually used as lithium contained positive electrode material.

In charging process of full cell configuration, de-intercalation of lithium ion in interstitial site of positive electrode material occurs. Therefore, in full cell case, lithium ion moves from positive to negative electrode in charging process of cell, and at discharging reaction of cell, reverse reaction of charging appears. In short, lithium ion moves like rocking-chair, and it is original concept of "rocking-chair model"[1]. The mechanism of the lithium ion battery is shown in figure 1.[2]

### 2.1.2. Characteristics of lithium ion batteries

Lithium ion battery system has tremendous advantage with its high energy density. Energy density of cell is calculated by multiplying working voltage and capacity of full cell. Therefore, to get maximized advantage of lithium ion battery system, using high voltage positive electrode with low voltage negative electrode material is needed. Also, lithium is the lightest atom except hydrogen and helium, therefore, specific energy and rate capability of battery system is expectable.

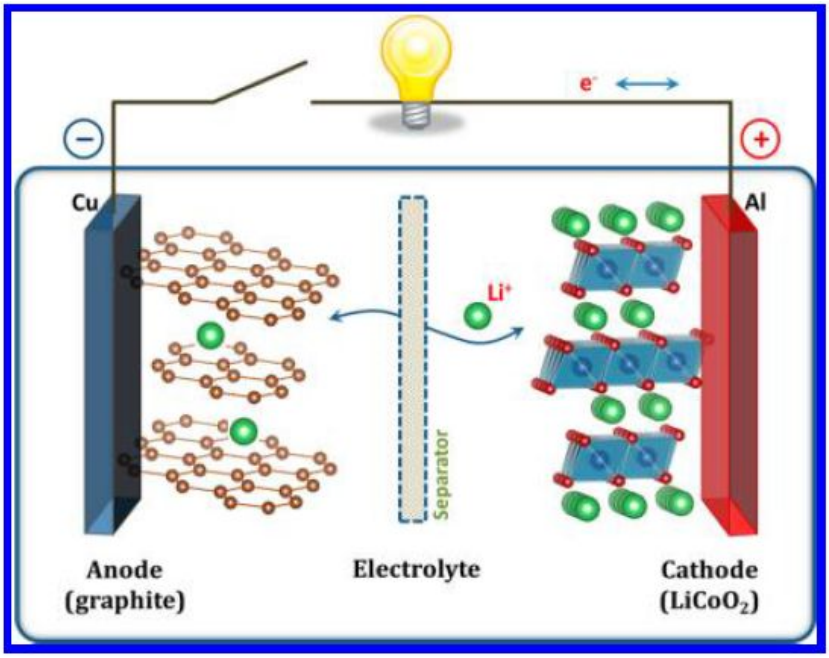


**Figure 1**. Schematic illustration of the first Li- ion battery (LiCoO2/Li+electrolyte/graphite)

## 2.2. Components of lithium ion batteries

Lithium ion secondary battery system is composed of four essential components, negative and positive electrode, separator for inhibiting physical shortage and lithium ion conducting electrolyte.[3] In generally, positive electrode materials have lithium ion sources of full cell. Therefore designing full cell capacity is almost determined by positive electrode materials. In this chapter, electrode materials and electrolytes are reviewed shortly.

### 2.2.1. Negative electrode materials

Initially, commercialized lithium secondary battery uses lithium metal as negative electrode material. Lithium metal has the highest capacity than any other negative electrode materials. Furthermore, by using lithium source included negative electrode material, selection pool of positive electrode materials have more easily than non-included case.[4]

However, lithium dendrite formation during cycling and internal-shortage by generated dendrites show safety problem with joule heating in the cell. This

phenomenon demonstrates thermal runaway.[5-8] From these reasons, alternative negative electrode materials are suggested. i.e. carbonaceous material, metal oxide or sulfide material and alloying reaction based active materials.[9-13]

### 2.2.1.2. Carbon based negative electrode

Most used negative electrode material is carbon based negative electrode materials, especially graphite. Graphite expresses its capacity below 0.3 V (*vs*, $Li/Li^+$)[9]. Also, lithium ion is intercalated and stored between grapheme layers, so stability of structure is observed. From these reasons, by using graphite as negative material for lithium ion battery, high energy density with long-term cyclceability is possible.

Intercalation and de-intercalation of lithium ion at graphite is expressed as below equation.

$$Li^+ + e^- + C_6 \leftrightarrow LiC_6 \qquad (1)$$

In charging process, carbon surpasses reduction of itself with lithium ion intercalation and vice versa at discharging process.

Carbonaceous materials can be classified as three large groups. Graphitic

carbon, graphitizable carbon and non-graphitizable carbon are those groups. Graphitic carbons have almost so structure defects with highly developed layered structure. Therefore, its capacity is determined by number of interstitial site. Graphitizable carbon, especially soft carbon, have layer characteristics with short-range order so, by temperature treatment, graphite structure can be generated. Non-graphitizable carbon have characteristics of cannot be graphitized by temperature treatment. Lithium storage sites of this class are not defined by trivial interstitial number of carbon structure. Therefore, high reversible capacity is desirable. In general, graphite shows specific capacity of 372 mA h $g^{-1}$, and hard carbon shows nearly 500 mA h $g^{-1}$. This is because stored lithium in hard carbon is at meso or micro pore of synthesized carbonaceous material. From this characteristic, large irreversible capacity is observed at hard carbon.[1, 14]

### 2.2.1.3. Alloy reaction based negative electrode

To prevent dendrite generation by using lithium metal, lithium-metal alloy system is introduced for high capacity electrode material. These alloy based

materials are Si, In, Pb, Ga, Ge, Sn, Al, Bi, Sb and generalized equation is expressed as below.[10, 15-20]

$$xLi^{+} + xe^{-} + M \leftrightarrow Li_xM \quad (2)$$

Alloy based negative electrode materials show high reversible capacity with acceptable working voltage. However, large volume change with lithiation, de-lithiation demonstrates poor cycleability and it is bottle-neck for commercialization.[18]

### 2.2.1.4. Transition metal oxides

Lithiation mechanism of metal oxide is deviated with metal-oxygen bond strength in metal oxide structure.[21]

$$MO_x + yLi^{+} + ye^{-} \leftrightarrow M_yLiO_x \quad (3\text{-}1)$$

$$MO_x + 2xLi^{+} + 2xe^{-} \leftrightarrow M + 2xLi_2O \quad (3\text{-}2)$$

Several examples for insertion reaction type metal oxide negative material is

$TiO_2$, $V_2O_5$, and $Li_4Ti_5O_{12}$[11, 22, 23]. Especially, $Li_4Ti_5O_{12}$ shows high rate capability with 3-d diffusion pathway via spinel structure. However, theoretical capacity of LTO is restricted by 175 mA h $g^{-1}$ with its interstitial sites. Also it has poor electronic conductivity and high working voltage with ~1.5 V. Therefore, it is defects for commercializing this material.

Second mechanism of transition metal oxide is conversion reaction, proposed by Tarascon.[12] Conversion reaction type materials show high reversible capacity by its mechanism. Mechanism is; lithium ion is reacted with oxygen atom of metal oxide and forming lithia and transition metal. Therefore, with number of oxygen in transition metal oxides, storage amounts of lithium ion are dramatically raised.[12, 13, 21, 24-26]

### 2.2.2. Positive electrode materials

By using non-lithium contained negative electrode material, it is essential to applying lithium ion contained positive electrode materials with high working voltage[27]. Previously reported positive electrode materials with lithium source have restricted capacity via its limited interstitial sites. This chapter briefly handles these materials.

### 2.2.2.1. Positive electrode with layered structure

Generalized form of positive electrode materials with layered structure is $LiMO_2$ (M= V, Cr, Fe, Co, and Ni). In specific example, $LiCoO_2$, show excellent reversibility with electrochemical lithiation and de-lithiation with 0.5 lithium ion. It is only half of its theoretical capacity, and this characteristic restricts its application of high voltage positive electrode material.[1, 14, 28] To handle this issue, $Al_2O_3$ coating and doping other transition metals is applied.

$LiNiO_2$ expresses high capacity with acceptable voltage. However, similar ion diameter with lithium and nickel, cation mixing problem is severe at synthesis process and it is one reason for degradation of active material based nickel ion.[29, 30]

### 2.2.2.2. Positive electrode with spinel structure

Spinel based positive electrode materials have general expression of $LiM_2O_4$. Especially, $LiMn_2O_4$ is probable positive electrode material for ESS application by its low cost and easy preparation. However, by structural instability via manganese ion and HF formation by $LiPF_6$ based electrolyte shows degradation

performance of full cell cycle. Manganese ion with 3+ oxidation state shows Jahn-Teller distortion at octahedral site and from this, z-elongation is observed. Therefore, LMO shows manganese ion dissolution by this structure instability. To prevent this transition metal dissolution, modification of oxidation state of manganese ion is preceded. By introducing other transition metals or lithium is one of those situations.[31-33]

### 2.2.2.4.. Positive electrode with olivine structure

Olivine structure, e.g. $LiFePO_4$, is environment friendly and economic material. Olivine structure has one dimensional pathway of lithium ion and from this feature, sluggish kinetic of lithium diffusion is bottle-neck for this system. To handle this issue, size controlling and transition metal doping is applied for this system.[34-37]

### 2.2.3. Electrolytes, additives and passivation films

#### 2.2.3.1. Organic solvents and lithium salts for electrolyte solution

To achieve high energy density secondary battery system, organic solvent is applied for electrolyte of lithium ion batteries. Organic solvent, especially carbonate based electrolyte is used for solvent, because it has characteristics of wide electrochemical stability window and high dielectric constant of solvents. Needed features of electrolyte for lithium ion battery system are high lithium ion conductivity and high polarity for fine solvation of lithium salts.

Selection of proper solvent is also important. One possible example is using graphite and propylene carbonate solvent used electrolyte case. Propylene carbonate (PC) was anticipated as most-probable carbonate solvent for lithium ion secondary battery system. One reason for using PC is its high dielectric constant and second reason is its physical property, especially freezing point. However, in graphite negative electrode, interfacial problem was observed. Co-intercalation and decomposition after co-intercalation of PC are defined reasons for that drawback. Therefore, by using PC as solvents for electrolyte solvents of graphite, inevitable defects are attended. From these reasons,

electrolyte solvent for lithium ion battery system is generally ethylene carbonate (EC).

However, viscosity and freezing point of EC are deficient points of electrolyte solvent. To handle these issues linear carbonate solvents are added as co-solvents, i.e. dimethyl carbonate, diethyl carbonate. By introducing these solvents, EC maintains its liquid form at room temperature and viscosity enhancement is desirable. In short, electrolyte solvents of lithium ion battery are generally almost co-solvent system, more specifically, EC and linear carbonate combination.

Proper lithium salts for electrolyte are also needed for fine operation of cell. For example, LiTFSI case, aluminium corrosion is observed at positive current collector. Therefore, it is essential to apply proper salts for full cell configuration. $LiPF_6$ salt is generally used for lithium salt. $LiPF_6$ have acceptable stability in room temperature and easily dissociated in used solvents as lithium ion and $PF_6^-$ due to large differences of ion size between lithium ion and $PF_6^-$. And also same reason with easy dissociation of cation and anion, lithium transference number is nearly identical with size of $PF_6^-$. Other salts are applied for lithium ion battery system, e.g. $LiBF_4$, $LiClO_4$ and etc. However, perchlorate salts have potential explosive problem, so commercialization of that electrolyte is not a simple problem.

Therefore, to get maximized performance of lithium ion battery system, selecting of proper solvents and lithium salt is needed.

# 3. Experimental

## 3.1 Cell construction

### 3.1.1 Preparation of composite electrode

$LiNi_{0.5}Co_{0.2}Mn_{0.3}O_2$ (NCM 523) was used as active material. Weight ratio of fabricated composite electrode of the active material, the conducting agent(Super P) and binder(PVdF(poly(vinylidenefluoride), KF1300) was 90:5:5. Initially, powder of active material and conducting agent were mixed and dried at 120°C convection oven. The dried mixture was blended with *N*-methylpyrrolidone (NMP) and PVdF. After slurry was coated on Al foil (10 μm), the composite electrode was dried at 120°C convection oven for a while. Fabricated composite electrode was pressed about 80 percent of its previous thickness. After punching composite electrode about diameter of 11 mm, the electrode was dried overnight at vacuum.

### 3.1.2 Fabrication of coin-type cell

Coin type cells (2032 size, Hohsen) were assembled in Ar filled glove box.

Composition of coin cell was composite electrode, separator (PP/PE/PP) and lithium metal as counter and reference electrode with electrolyte, 1 *M* $LiPF_6$ in EC:DEC (*v*/*v*=1:1) and 1 *M* $LiPF_6$ in EC:DEC (*v*/*v*=1:1) with 2wt% VC and 1 *M* $LiPF_6$ in EC:DEC (*v*/*v*=1:1) with 2wt% PS were used as electrolyte solution.

## 3.2 Electrochemical characterization

### 3.2.1 Galvanostatic charge/discharge experiment

To soak electrolyte with composite electrode and separator, the assembled half cells were rested with 12 hours at room temperature. After wetting process, galvanostatic charge and discharge experiments were carried out using battery cycler (wonatech inc.) after formation. Formation of fabricated cells was preceeded with voltage range of 3.0 ~ 4.7 V with 3 cycles, 0.2 *C* constant current (CC) and at charge end, 4.7 V constant voltage (CV) step was applied with 0.05 *C* current cut-off. After stabilizing passivation film, cycle performance was tested with voltage range of 3.0 ~ 4.7 V with 70 cycles, 0.5 *C* constant current (CC) and at charge end, 4.7 V constant voltage (CV) step was applied with 0.1 *C* current cut-off. High temperature (60 $^{o}$C) cycling was

carried out after thermal equilibrium, as 30 minutes rest, and same electrochemical condition is applied with 25 $^{o}$C cycling.

### 3.2.2 Linear sweep thermammetry(LSTA) test

After forming passivation film at room temperature, the coin cell was stabilized during 5 hours at constant applied 4.7 V CV. After stabilization temperature sweep was applied with 0.1 $^{0}$C min$^{-1}$, and the range of temperature was 25~80 $^{0}$C. In temperature sweep step, anodic current was collected as function of temperature.

### 3.2.3 AC Impedance test

After charging process at 4.7 V, AC impedance test was performed by using Chi 660B. The range of frequency is from 5 mHz to 100 kHz.

## 3.3 Analysis via spectroscopic methods

### 3.3.1 X-ray diffraction pattern analysis (XRD)

X-ray diffraction pattern is collected by XRD instruments (Brucker, D8) with 2θ range of 10 ~ 80 degrees. After collecting pattern, JCPDS is used for assigning crystal structure.

### 3.3.2 Field Emission Scanning Electron Microscopy (FE-SEM)

FE-SEM (JEOL JSM-6700F) was used for identify the particle of active material.

### 3.3.3 X-ray photoelectron spectroscopy (XPS)

At the end of charging, the coin cell was disassembled in a glove box, and washed with diethyl carbonate (DEC) to eliminate the lithium salt and the electrolyte. After drying residual DEC solvent, a piece of electrode moved from

a glove box into an instrument chamber. The binding energy was calibrated by the C 1s peak at 285.0 eV, which was obtained from hydrocarbon contamination.

# 4. Results and Discussions

## 4.1 Characterization of active material

$LiNi_{0.5}Co_{0.2}Mn_{0.3}$ (NCM523) is a promising positive electrode material for lithium secondary batteries with its high capacity and acceptable working voltage. It is composed of three transition metal elements of nickel, cobalt, and manganese. Ni ions give characteristic of high capacity, Mn ions give economical advantage and Co ions improve layered characteristics of active material. However, only Ni and Co ions involve redox reaction as $Ni^{2+/4+}$ and $Co^{3+/4+}$ redox couples. Therefore, Mn ions stays in 4+ oxidation state with non Jahn-teller distorsion involved structure. NCM 523 is more stable than $LiNi_{1/3}Co_{1/3}Mn_{1/3}O_2$ (NCM333) by reducing number fraction of Co ions. Furthermore, NCM 523 is easily influenced by surface characteristic because it contains higher number fraction of Ni ions than NCM 333.

Figure 2 shows X-ray diffraction (XRD) pattern of used active material, and this pattern shows used sample has well-developed layered structure. Figure 3 shows FE-SEM image of NCM 523. Microscope image demonstrates used sample has spherical structure with 10 μm particle size.

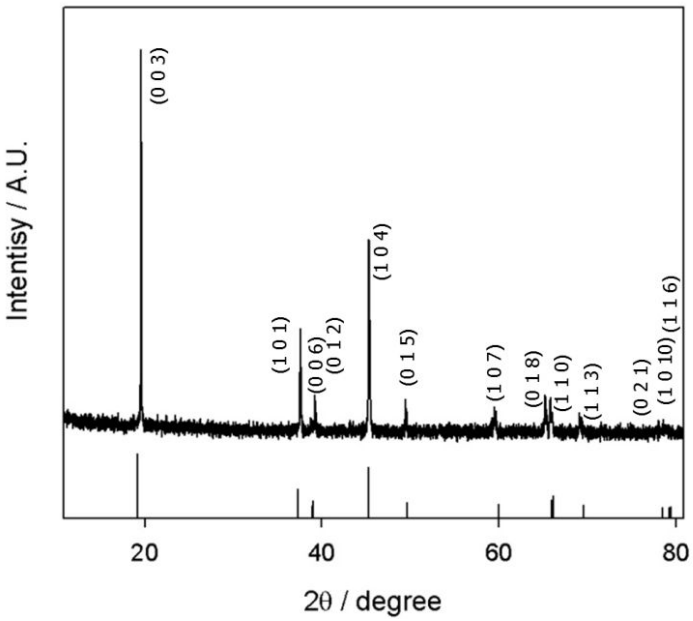


**Figure 2**. XRD patterns of $LiNi_{0.5}Co_{0.2}Mn_{0.3}O_2$

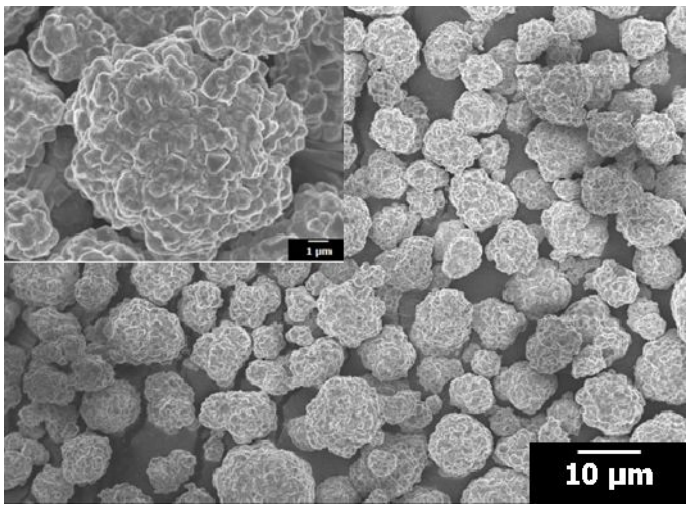


**Figure 3**. FE SEM image of $LiNi_{0.5}Co_{0.2}Mn_{0.3}O_2$

## 4.2 Formation of passivation film

To see LSTA tool is feasible for facile identification of long-term cycle performance, two different known additives and bare electrolyte solution are used for identification. VC (Vinylene Carbonate), predicted as having poor cycleability in high temperature and voltage[38], and PS (Propane Sultone), expected as showing good cycleability in same condition[39]. And to see passivation film is generated at formation cycle of NCM 523 electrode, differential capacity plot analysis is preceded. Figure 4 shows differential capacity plots of three samples. In 1st cycle of formation, VC and PS 2wt% added electrolyte used sample shows strong oxidation peak at 4 ~ 4.3 voltage region. However, in bare electrolyte case, there is no strong oxidation peak is defined after redox reaction of active material. It is due to characteristic of used positive electrode material. NCM 523 expresses its capacity with continuous voltage-rise or decay in voltage profile, therefore oxidation reaction of electrolyte solution is not clear in differential capacity plot. Nevertheless, formation of passivation film is confirmed by comparing coulombic efficiency of 1st and 2nd cycle of active material formation. 2nd cycle shows much higher coulombic efficiency than 1st cycle, because further electrolyte decomposition is suppressed by passivation film

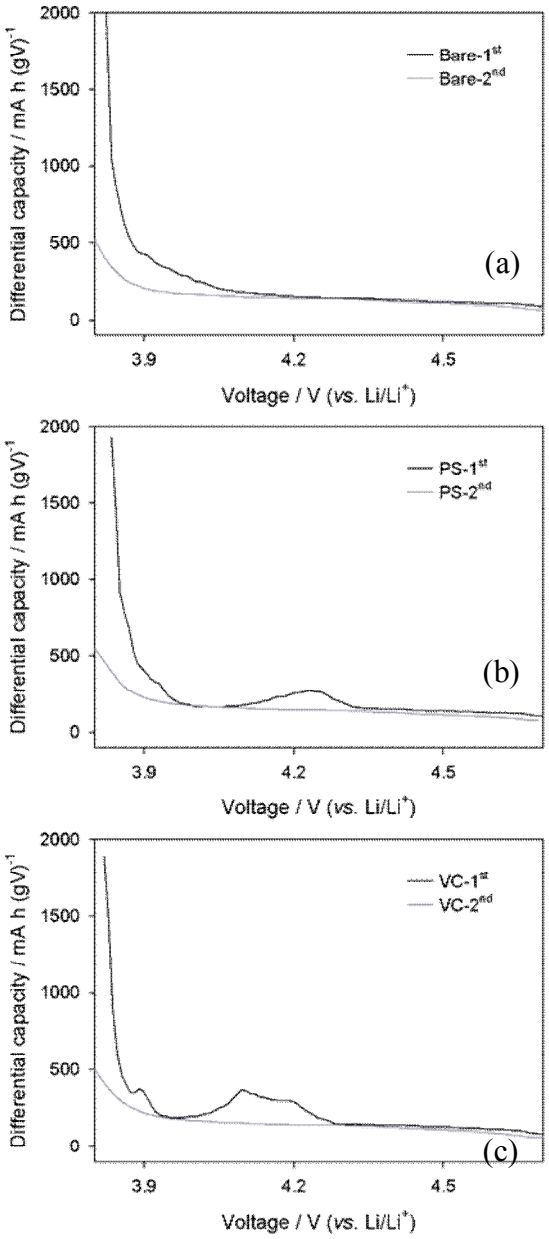


**Figure 4**. Differential capacity plots of formation cycles of (a) non-additive (b) 2 *wt.* % PS and (c) 2 *wt.* % VC with 1 *M* $LiPF_6$ in EC:DEC (1:1=*v*/*v*) electrolyte

## 4.3 Linear sweep thermammetry (LSTA) test

Linear sweep thermammetry(LSTA) is measuring anodic or cathodic current during temperature sweep at constant applied voltage. This method can estimate amount of reaction occurred at working electrode as a function of temperature. Furthermore, it can measure flowed current during linearly swept temperature from 25 $^{0}$C to 80 $^{0}$C with a ramp of 0.1$^{0}$C min$^{-1}$, So it is very fast and simple to get overall current data with given temperature region.

In this study, LSTA experiment was performed after formation of passivation film at room temperature and stabilization of working electrode at given voltage. By doing this, we can confine the origin of the anodic current of LSTA test. One is further oxidation of formed passivation film and other one is additional side reaction, especially, electrolyte decomposition by destruction of passivation film with temperature rise. Therefore, we can define amounts of flowed current are directly correlated to passivation film stability. Thus, if we want to know stability of several samples with different passivation film, it is easily compared with current flowing measured by LSTA.

Also, in general case, stability of passivation film at high temperature is important to performing fine cycleability. Figure 5 shows conventional behavior of passivation film at high temperature cycling. During formation step,

passvation film will generate on active material at room temperature (25 $^{0}$C). If stability of passivation film is not enough durable to prevent decomposition of passivation film at high temperature, further electrochemical decomposition of electrolyte will occur. Therefore, degradation of capacity will occur. By LSTA method, we can get stability information of passivation film easily, and it is directly correlated to prediction of cycle performance of battery system. Therefore, LSTA method can be one of important method for testing electrolyte solution of battery system, facile and easily.

Figure 6 shows specific current-temperature plots from LSTA method. LSTA method is performed after constant voltage of 4.7 V reducing effect of residual lithium ion at applied voltage and then temperature sweep is preceded. At room temperature (25 $^{0}$C), amount of anodic currents between three samples show no difference. However, data collected at high temperature (60 $^{0}$C), the amount of anodic current of VC added sample is the largest and bare, PS in sequence. This tendency is same as we predicted at the point of designing this experiment with additive selection.

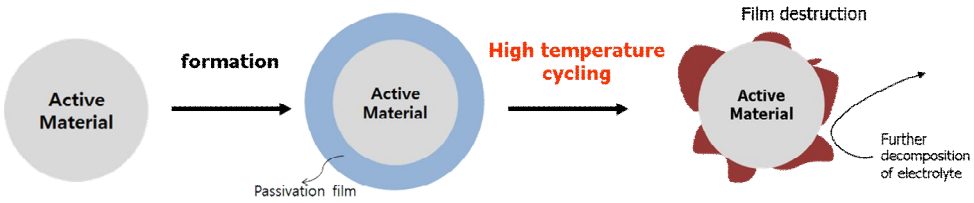


**Figure 5.** Schematic diagram of passivation film at high temperature cycling

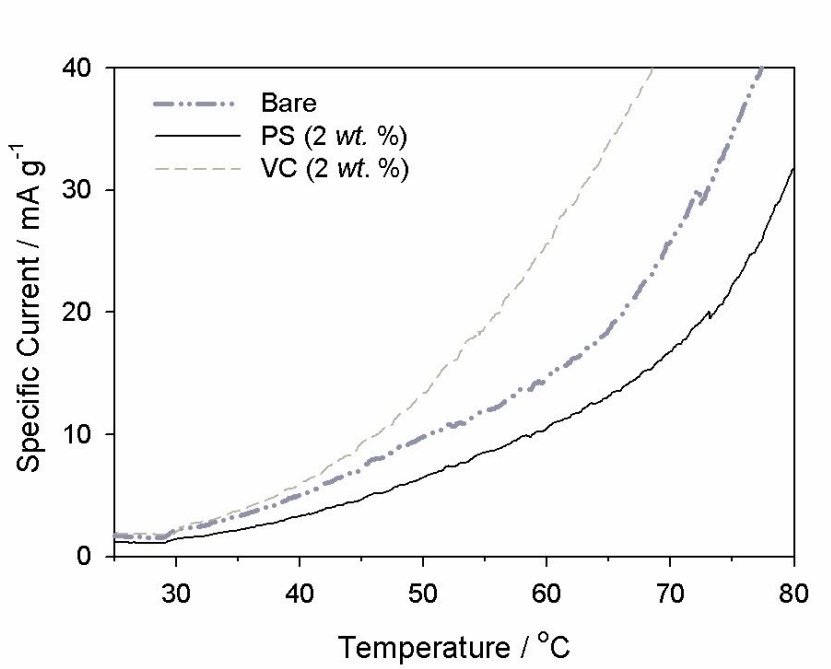


**Figure 6**. Measured oxidation specific current with 0.1 $^{0}$C min$^{-1}$ temperature sweep at 4.7 V constant voltage

## 4.4 Validate LSTA as tool for predicting cycleability

### 4.4.1 Room temperature performance

#### 4.4.1.1 Comparison of cycle performance

To define LSTA is possible tool for predicting long-term cycle performance of fabricated cell, real cycling was performed. In room temperature case, measured currents by LSTA method show no meaningful difference. Therefore, it is easy to predict cycle performances of three samples are similar. Figure 7 shows performed cycleabilities of three samples. As we can see in figure 7, predicted tendency is matched with real long-term cycle performances of three samples.

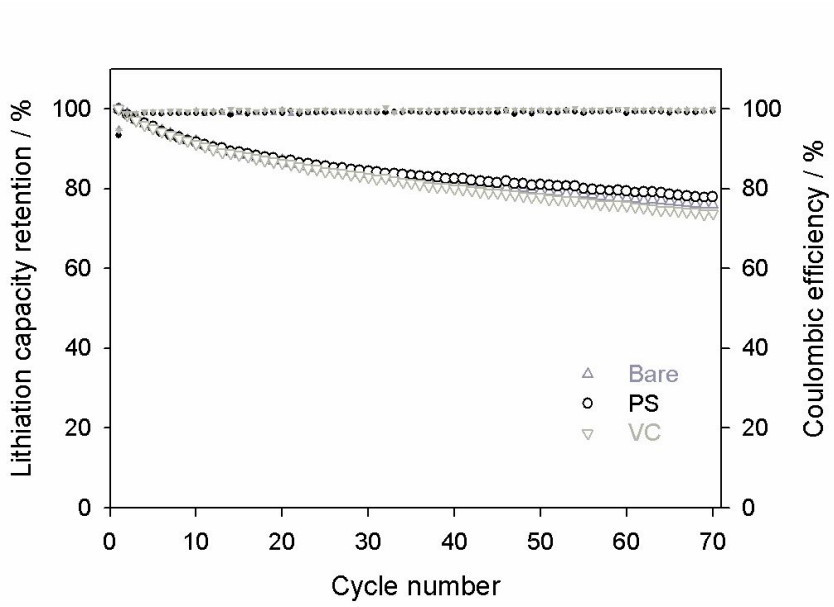


**Figure 7**. Discharge capacity retention and coulombic efficiency of at 25 $^{0}$C with 0.5 *C CC* and 4.7 V *CV* with 0.1 *C* current cut-off

### 4.4.1.2 Investigation of dependencies between cycle life and passivation film properties

#### 4.4.1.2.1 Differential capacity plot analysis

Cycleabilities of three samples are similar as we predicted by LSTA experiment, however, it is needed to define this phenomenon is really due to surface characteristics. Therefore, we attempt to confirm increments of polarization after cycling are similar with three samples. Figure 8 shows de-lithiation differential capacity plots of $1^{st}$ and $50^{th}$ cycle of three samples. Oxidation peaks at 3.7 ~ 3.9 V region represent redox reaction of active material. By comparing oxidation peak voltage at $1^{st}$ cycle and $50^{th}$ cycle, polarization can be measured. As we can see in figure 8, polarization increments among three samples are similar. In short, it can be easy to say similar increment of resistance takes place with three samples. . Table 1 demonstrates its specific values. And to see further specified resistance, AC impedance analysis is preceeded.

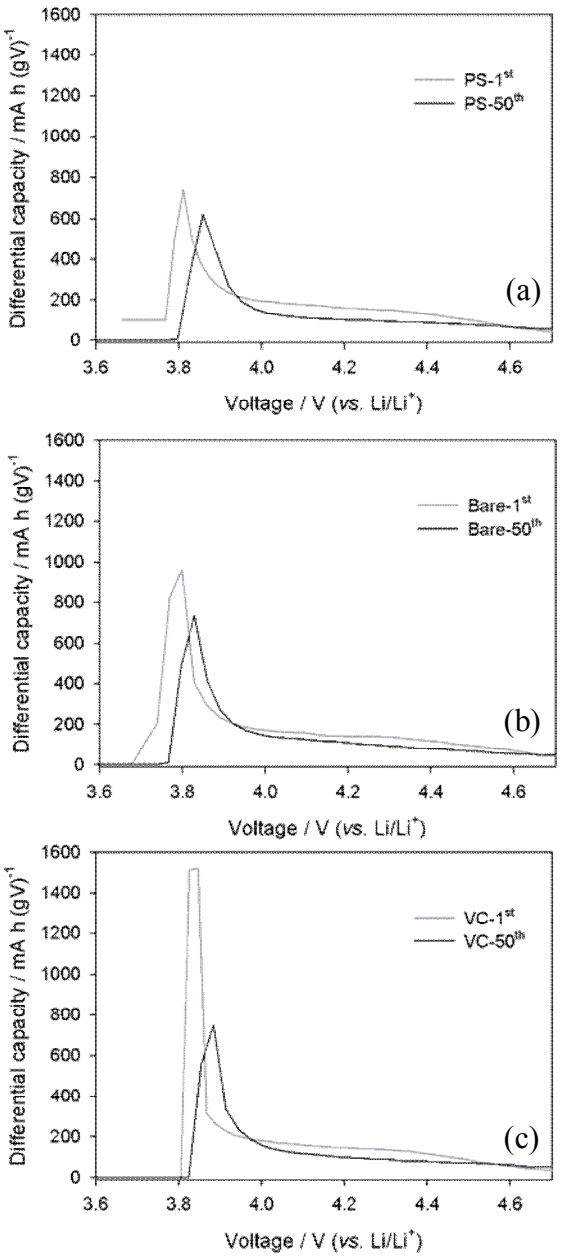


**Figure 8**. Differential lithiation capacity plot of 1$^{st}$ and 50$^{th}$ cycle at 25 $^0$C of (a) 2 *wt.* % PS (b) non-additive and (c) 2 *wt.* % VC with 1 *M* $LiPF_6$ in EC:DEC (1:1=*v/v*) electrolyte

| Electrolyte | Increment of reaction voltage / mV |
|---|---|
| 2 *wt.* % PS | 48.7 |
| Non-additive | 30.2 |
| 2 *wt.* % VC | 48.0 |

**Table 1.** Polarization increment comparison at 25 $^{0}$C cycling with additive difference

#### 4.4.1.2.2 AC impedance analysis

Figure 9 shows nyquist plots of three samples with 1st and 50th cycle. As previously reported, 1st semicircle of nyquist plot represents resistance of SEI (solid electrolyte interphase) or passivation film, so we can compare film resistance by AC impedance method.

As we can see in figure 9, there is similar rises of surface film resistance. This phenomenon is well-agreed with predicted LSTA data. LSTA shows similar current amounts with three samples and this tendency is appeared at cycle performance of VC, PS, and bare electrolyte. Further analysis of resistance film of three samples also represents this trends and it can be a possible evidence for LSTA can be act as tool for predicting long-term cycle performance.

### 4.4.1.3 Schematic diagram

As we described previous chapters with tendency with polarization increment and rises of surface film resistance, schematic diagram of three samples is also applicable. Figure 10 shows schematic diagram of three samples at room temperature cycling. After cycling, no meaningful difference of film thickness may be observed among three samples. These situations are demonstrated at figure 8 as schematic diagram

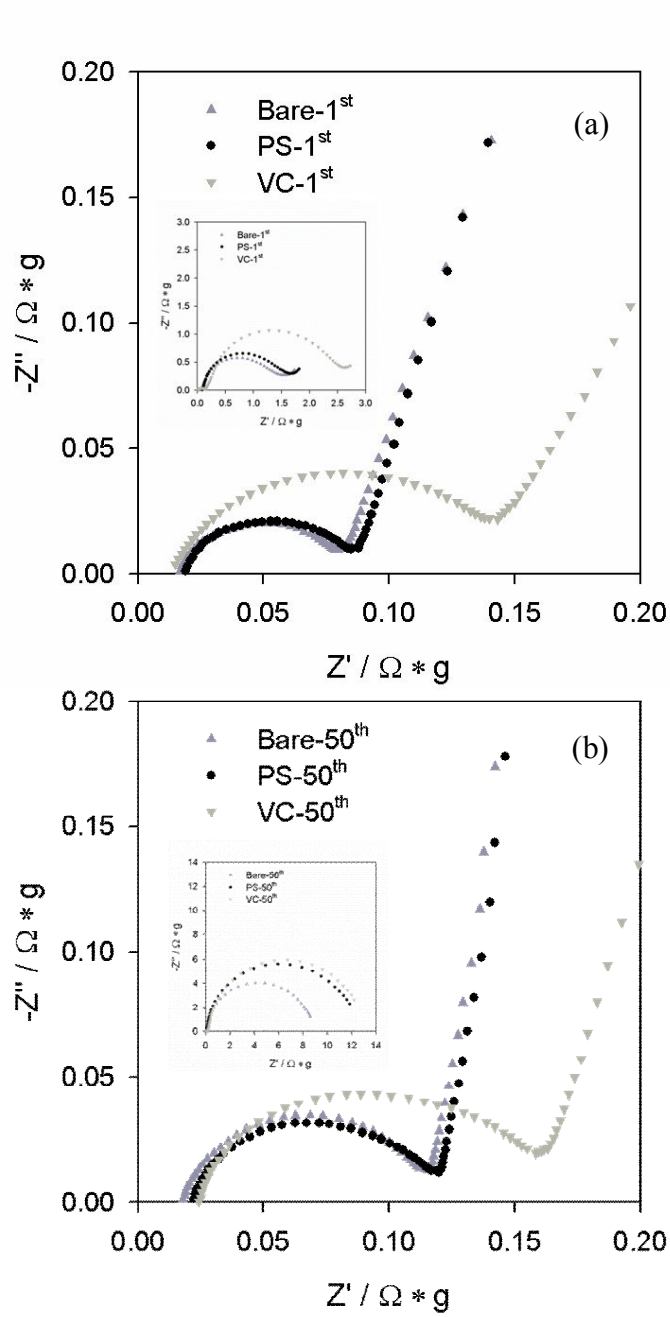


**Figure 9.** Nyquist plots of non-additive, 2 *wt.* % PS and 2 *wt.* % VC with 1 *M* $LiPF_6$ in EC:DEC (1:1=*v/v*) electrolyte (a) after formation and (b)$50^{th}$ cycle at 25 $^0$C

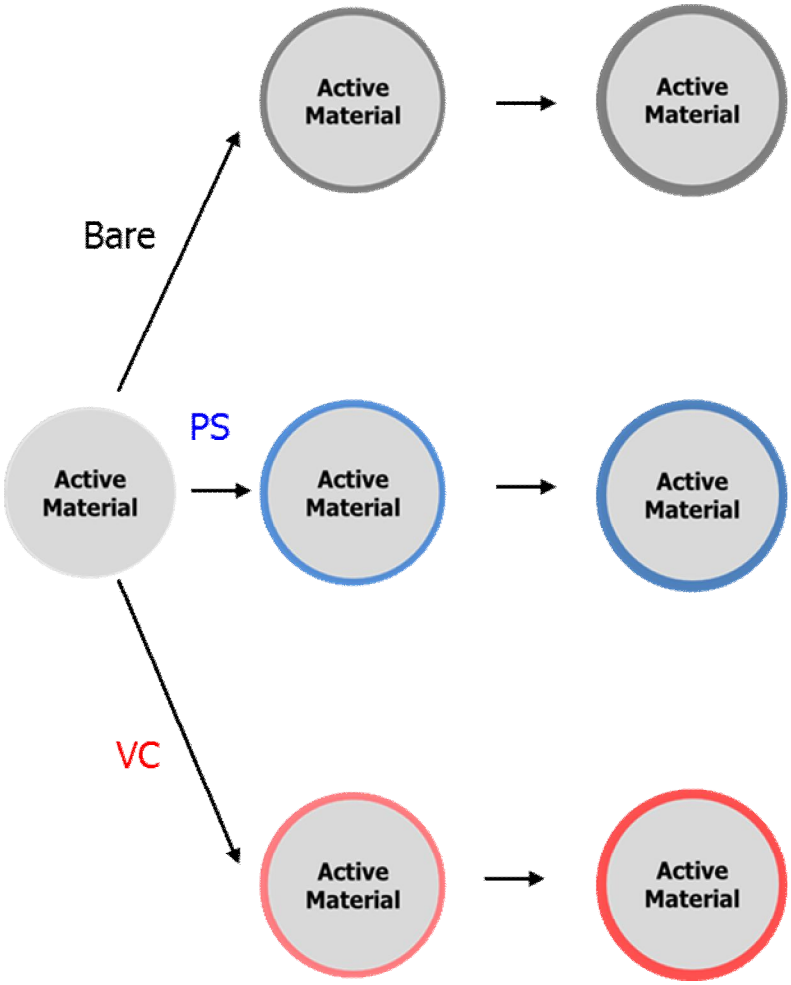


**Figure 10.** Schematic diagram of passivation film (a) after formation and (b)50$^{th}$ cycle at 25 $^{0}$C

### 4.4.2 High temperature ($60^0$C) performance

#### 4.4.2.1 Comparison of cycle performance

To define LSTA is possible tool for predicting long-term cycle performance of fabricated cell, real cycling was performed also at high temperature. In room temperature case, measured currents by LSTA method show no meaningful difference, but in high temperature case, amounts of oxidation current is VC, bare, and PS with descending order. Therefore, it is easy to predict cycle retentions of three samples are VC, bare, and PS in sequence. Figure 11 shows performed cycleabilities of three samples. As we can see in figure 11, predicted tendency is matched with real long-term cycle performances of three samples.

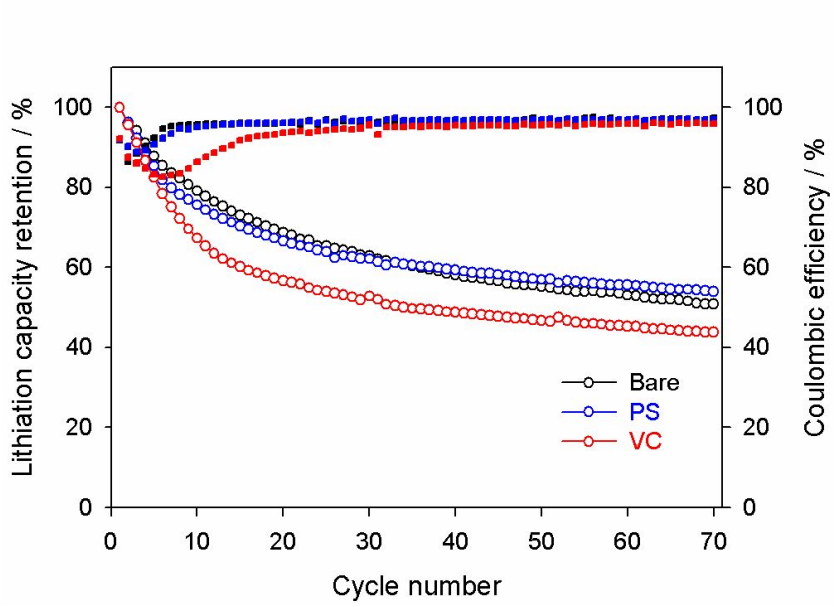


**Figure 11**. Discharge capacity retention and coulombic efficiency of  at 60 $^{0}$C with 0.5 *C CC* and 4.7 V *CV* with 0.1 *C* current cut-off

### 4.4.2.2 Comparison of polarization

#### 4.4.2.2.1 Differential capacity plot analysis

Cycleabilities of three samples shows meaningful difference with oxidation current, so it is needed to define this phenomenon is really due to surface characteristics. Therefore, we attempt to confirm increments of polarization after cycling with three samples. Figure 12 shows de-lithiation differential capacity plots of $1^{st}$ and $50^{th}$ cycle of three samples at high temperature. In differential capacity plots of three samples, oxidation peaks at 3.7 ~ 4 V region represent redox reaction of active material. By comparing oxidation peak voltage at $1^{st}$ cycle and $50^{th}$ cycle, polarization can be measured. As we can see in figure 12, amounts of polarization increments among three samples show VC, bare, and PS in sequence. In short, it can be easy to say difference amounts of resistance increment takes place with three samples. Table 2 demonstrates its specific values. And to see further specified resistance, AC impedance analysis is preceded.

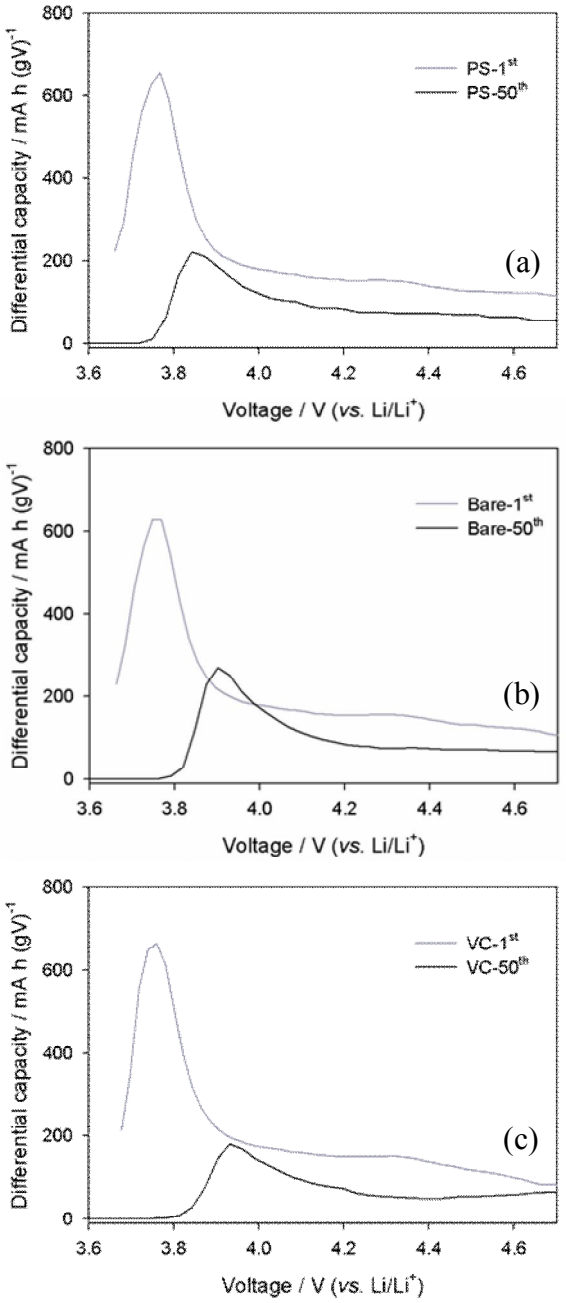


**Figure 12**. Differential lithiation capacity plot of 1st and 50th cycle at 60 $^0$C of (a) 2 *wt.* % PS (b) non-additive and (c) 2 *wt.* % VC with 1 *M* $LiPF_6$ in EC:DEC (1:1=*v/v*) electrolyte

| Electrolyte | Increment of reaction voltage / mV |
|---|---|
| 2 *wt.* % PS | 74.8 |
| Non-additive | 143.3 |
| 2 *wt.* % VC | 172.4 |

**Table 2.** Polarization increment comparison at 60 $^{0}$C cycling with additive difference

#### 4.4.2.2.2 AC impedance analysis

Figure 13 shows nyquist plots of three samples with 1st and 50th cycle at high temperature. As previously reported, 1st semicircle of nyquist plot represents resistance of SEI (solid electrolyte interphase) or passivation film, so we can compare film resistance by AC impedance method.

As we can see in figure 13, different amounts of increment of surface film resistance is observed. This phenomenon is well-correspond to predicted LSTA data, especially amounts of oxidation current. LSTA shows different degree of oxidation currents with three samples, VC, bare and PS in sequence, and this tendency is appeared at cycle performance of three samples. Further analysis of resistance film of three samples also represents this trends and it can be a possible evidence for LSTA can be act as tool for predicting long-term cycle performance. To see more precise factor for this resistance rise, XPS spectra analysis is applied for seeing thickness of surface film.

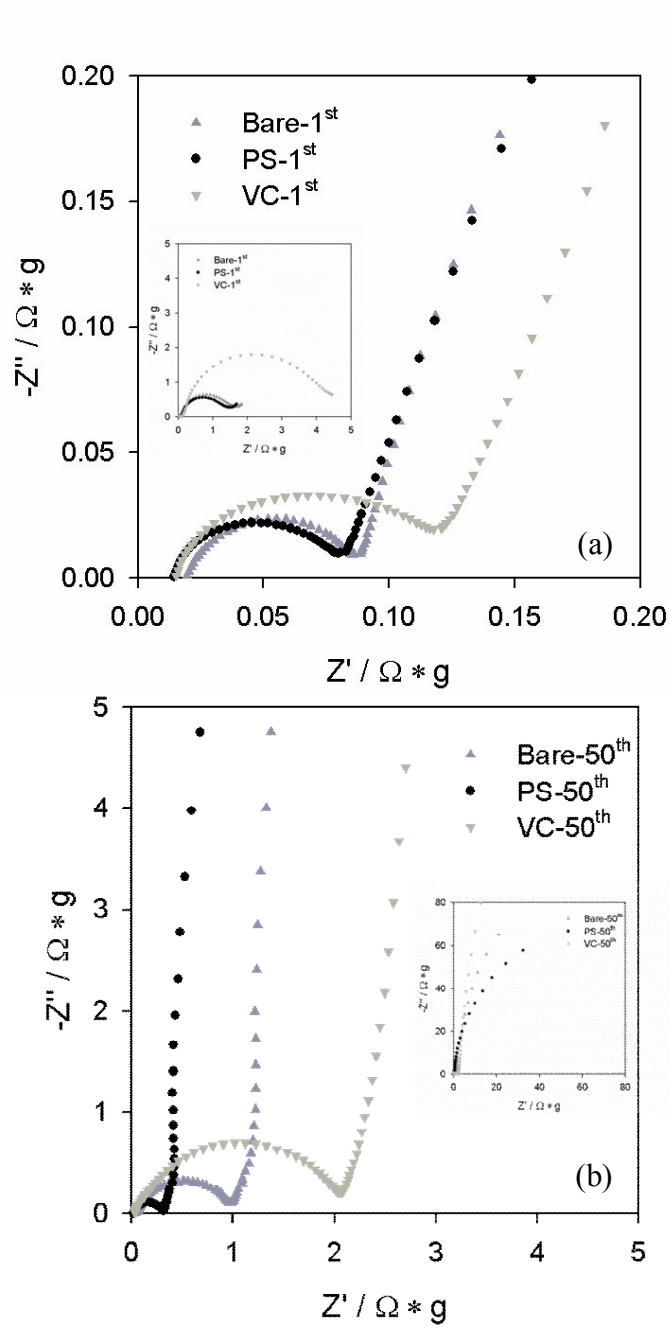


**Figure 13.** Nyquist plots of non-additive, 2 *wt.* % PS and 2 *wt.* % VC with 1 *M* $LiPF_6$ in EC:DEC (1:1=*v*/*v*) electrolyte (a) after formation and (b)$50^{th}$ cycle at 60 $^0$C

#### 4.4.2.2.3 XPS spectra

Figure 14 (a) shows XPS spectra of after formation cycle and (b) shows $100^{th}$ cycle at high temperature cycling. After $100^{th}$ cycling at high temperature, we can define increasing of surface film thickness is different with electrolyte solutions. Compare lattice oxygen intensity at O 1s spectra and nickel intensity at Ni 2p spectra, we can define thickness of three samples with additive variation after $100^{th}$ cycle[40]. As we can see in nyquist plots and table 2, quantity of film resistance of three samples is VC, bare electrolyte and PS with descending order.

This situation is also found at XPS spectra case. XPS spectra show lattice oxygen intensity with PS, bare, and VC in sequence at top-most of surface film, so we can infer thickness of film is the thinnest at PS and the thickest at VC. This phenomenon is as well as demonstrated at Ni 2p spectra. Intensity of Ni 2p spectra is the highest at PS and the lowest at VC. These features are well-agreed with cycleabilities, differential capacity plots and AC impedance data. Therefore, we verify that LSTA method is promising tool for predicting cycle performance with seeing relative surface film stability.

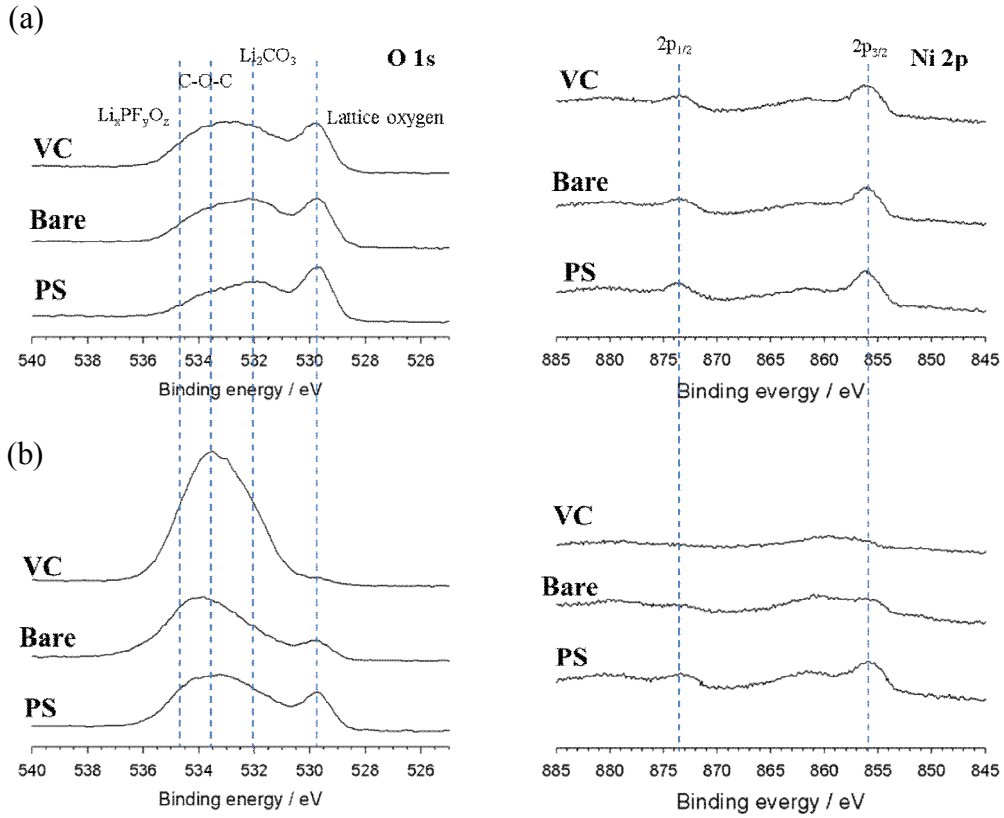


**Figure 14.** O 1s and Ni 2p XPS spectra of (a) after formation and (b) after 100$^{th}$ cycle at 60 $^{0}$C

### 4.4.2.3 Schematic diagram of high temperature cycling

As we described previous chapters with tendency with polarization increment and rises of surface film resistance, schematic diagram of three samples is also applicable. Figure 15 shows schematic diagram of three samples at high temperature cycling. In VC case, film thickness is dramatically increased with cycling, but in PS case, there is no significant thickness rise is observed after cycling. These situations are demonstrated at figure 15 as schematic diagram.

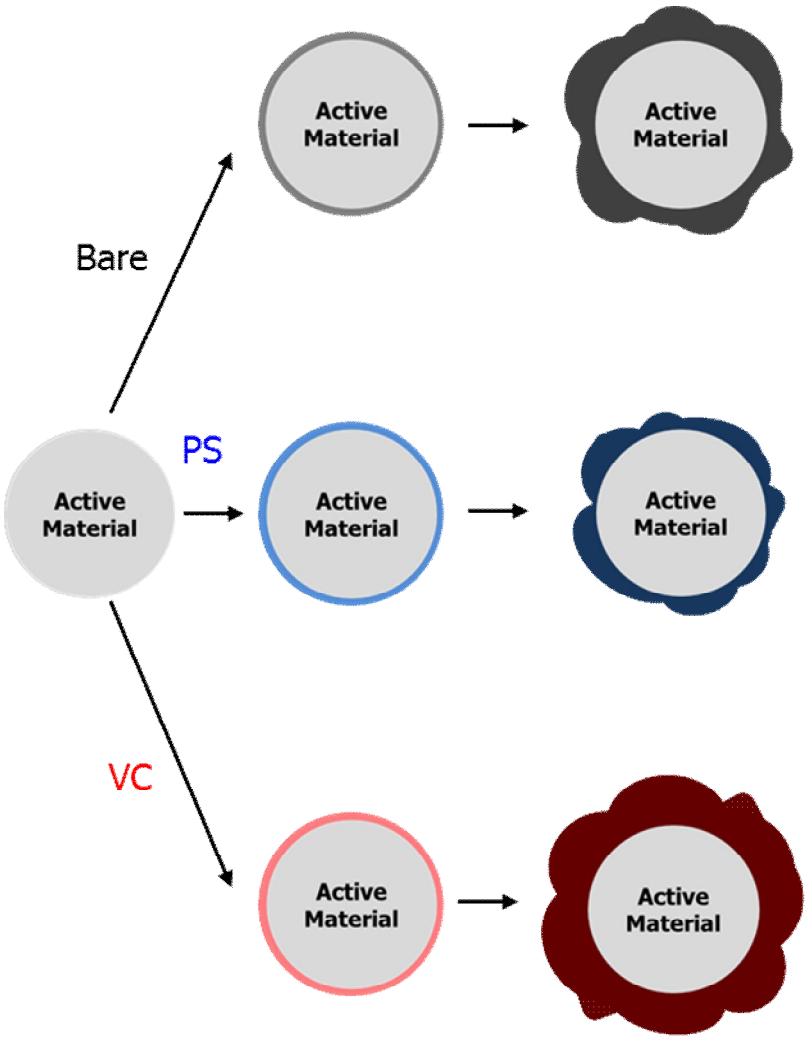


**Figure 15.** Schematic diagram of passivation film (a) after formation and (b)50$^{th}$ cycle at 25 $^{0}$C

# 5. Conclusions

In this study, we suggest LSTA as tool for predicting cycleability by measuring relative stability among different passivation films. Collected LSTA data after formation, in case of 25 $^0$C shows similar amount of oxidation currents with three samples and the case of 60 $^0$C demonstrates the highest current at VC and the lowest current at PS. And from cycle performance data, these two tendencies are also observed.

To define origin of degradation of cycle performance, differential capacity plot analysis is preceded for polarization analysis. From 25 $^0$C data, its results show there is almost same increment of polarization. However, in the case of 60 $^0$C, amounts of increment of polarization have trends with VC, bare electrolyte and PS in sequence. It shows polarization is reason of capacity degradation. To see further cause of polarization rise, AC impedance technique is applied. At 25 $^0$C, increased film resistance is almost same with three samples. Nevertheless, as we can predicted as polarization data, magnitude of film resistances after 60$^0$C cycling demonstrate VC, bare electrolyte and PS. XPS analysis is also preceded for further assigning this phenomenon. From lattice oxygen intensity from O 1s spectra and nickel intensity from Ni 2p spectra, VC has the thickest film and PS has the thinnest film among three samples. From this feature, we define

thickness of film after high temperature cycling affecting cycle performance of cell.

From these results, we can say that LSTA technique shows stability of surface film generated by variation of additives and it has direct correlation with cycle performance. Therefore, we can state that LSTA can be act as prediction tool for long-term cycleability.

# References


1. Winter, M., et al., *Insertion Electrode Materials for Rechargeable Lithium Batteries.* Advanced Materials, 1998. **10**(10): p. 725-763.
2. Goodenough, J.B. and K.-S. Park, *The Li-Ion Rechargeable Battery: A Perspective.* Journal of the American Chemical Society, 2013.
3. Whittingham, M.S. and T. Zawodzinski, *Introduction: Batteries and Fuel Cells.* Chemical Reviews, 2004. **104**(10): p. 4243-4244.
4. Xu, K., *Nonaqueous Liquid Electrolytes for Lithium-Based Rechargeable Batteries.* Chemical Reviews, 2004. **104**(10): p. 4303-4418.
5. Andersson, A.M., et al., *The influence of lithium salt on the interfacial reactions controlling the thermal stability of graphite anodes.* Electrochimica Acta, 2002. **47**(12): p. 1885-1898.
6. Andersson, A.M. and K. Edström, *Chemical Composition and Morphology of the Elevated Temperature SEI on Graphite.* Journal of The Electrochemical Society, 2001. **148**(10): p. A1100-A1109.
7. Lee, H.H., C.C. Wan, and Y.Y. Wang *Thermal Stability of the Solid Electrolyte Interface on Carbon Electrodes of Lithium Batteries.* Journal of The Electrochemical Society, 2004. **151**(4): p. A542-A547.

8. Zhang, S.S., *A review on electrolyte additives for lithium-ion batteries.* Journal of Power Sources, 2006. **162**(2): p. 1379-1394.

9. Noel, M. and R. Santhanam, *Electrochemistry of graphite intercalation compounds.* Journal of Power Sources, 1998. **72**(1): p. 53-65.

10. Winter, M. and J.O. Besenhard, *Electrochemical lithiation of tin and tin-based intermetallics and composites.* Electrochimica Acta, 1999. **45**(1-2): p. 31-50.

11. Poizot, P., et al., *From the vanadates to 3d-metal oxides negative electrodes.* Ionics, 2000. **6**(5): p. 321-330.

12. Poizot, P., et al., *Nano-sized transition-metaloxides as negative-electrode materials for lithium-ion batteries.* Nature, 2000. **407**(6803): p. 496-499.

13. Balaya, P., et al., *Fully Reversible Homogeneous and Heterogeneous Li Storage in RuO2 with High Capacity.* Advanced Functional Materials, 2003. **13**(8): p. 621-625.

14. Guyomard, D. and J.-M. Tarascon, *Rocking-chair or lithium-ion rechargeable lithium batteries.* Advanced Materials, 1994. **6**(5): p. 408-412.

15. Hochgatterer, N.S., et al., *Silicon/graphite composite electrodes for high-capacity anodes: Influence of binder chemistry on cycling stability.*

Electrochemical and Solid State Letters, 2008. **11**(5): p. A76-A80.

16. Guerfi, A., et al., *SiO(x)-graphite as negative for high energy Li-ion batteries.* Journal of Power Sources, 2011. **196**(13): p. 5667-5673.

17. McDowell, M.T., et al., *25th Anniversary Article: Understanding the Lithiation of Silicon and Other Alloying Anodes for Lithium-Ion Batteries.* Advanced Materials, 2013: p. n/a-n/a.

18. Ryu, J.H., et al., *Failure Modes of Silicon Powder Negative Electrode in Lithium Secondary Batteries.* Electrochemical and Solid-State Letters, 2004. **7**(10): p. A306-A309.

19. Jung, Y.S., et al., *Sn-Carbon Core-Shell Powder for Anode in Lithium Secondary Batteries.* Journal of The Electrochemical Society, 2005. **152**(7): p. A1452-A1457.

20. Jung, Y.S., K.T. Lee, and S.M. Oh, *Si-carbon core-shell composite anode in lithium secondary batteries.* Electrochimica Acta, 2007. **52**(24): p. 7061-7067.

21. Cabana, J., et al., *Beyond Intercalation-Based Li-Ion Batteries: The State of the Art and Challenges of Electrode Materials Reacting Through Conversion Reactions.* Advanced Materials, 2010. **22**(35): p. E170-E192.

22. Shu, J., *Study of the Interface Between Li4Ti5O12 Electrodes and*

*Standard Electrolyte Solutions in 0.0 – 5.0 V.* Electrochemical and Solid-State Letters, 2008. **11**(12): p. A238-A240.

23. Chen, Z., et al., *Titanium-Based Anode Materials for Safe Lithium-Ion Batteries.* Advanced Functional Materials, 2013. **23**(8): p. 959-969.

24. Débart, A., et al., *A Transmission Electron Microscopy Study of the Reactivity Mechanism of Tailor-Made CuO Particles toward Lithium.* Journal of the Electrochemical Society, 2001. **148**(11): p. A1266-A1274.

25. Laruelle, S., et al., *On the origin of the extra electrochemical capacity displayed by MO/Li cells at low potential.* Journal of the Electrochemical Society, 2002. **149**(5): p. A627-A634.

26. Poizot, P., et al., *Rationalization of the low-potential reactivity of 3d-metal-based inorganic compounds toward Li.* Journal of the Electrochemical Society, 2002. **149**(9): p. A1212-A1217.

27. Whittingham, M.S., *Lithium Batteries and Cathode Materials.* Chemical Reviews, 2004. **104**(10): p. 4271-4302.

28. Mizushima, K., et al., *LIXCOO2 "(OLESS-THANXLESS-THAN-OR-EQUAL-TO1) - A NEW CATHODE MATERIAL FOR BATTERIES OF HIGH-ENERGY DENSITY.* Materials Research Bulletin, 1980. **15**(6): p. 783-789.

29. Yamada, S., M. Fujiwara, and M. Kanda, *Synthesis and properties of*

*LiNiO2 as cathode material for secondary batteries.* Journal of Power Sources, 1995. **54**(2): p. 209-213.

30. Peres, J.P., et al., *The relationship between the composition of lithium nickel oxide and the loss of reversibility during the first cycle.* Journal of Physics and Chemistry of Solids, 1996. **57**(6–8): p. 1057-1060.

31. Tarascon, J.M. and D. Guyomard, *The Li1+xMn2O4/C rocking-chair system: a review.* Electrochimica Acta, 1993. **38**(9): p. 1221-1231.

32. Gummow, R.J., A. de Kock, and M.M. Thackeray, *Improved capacity retention in rechargeable 4 V lithium/lithium-manganese oxide (spinel) cells.* Solid State Ionics, 1994. **69**(1): p. 59-67.

33. Jang, D.H., Y.J. Shin, and S.M. Oh, *Dissolution of Spinel Oxides and Capacity Losses in 4 V Li / Li x Mn2 O 4 Cells.* Journal of The Electrochemical Society, 1996. **143**(7): p. 2204-2211.

34. Padhi, A.K., K.S. Nanjundaswamy, and J.B. Goodenough, *Phospho-olivines as Positive-Electrode Materials for Rechargeable Lithium Batteries.* Journal of the Electrochemical Society, 1997. **144**(4): p. 1188-1194.

35. Chung, S.-Y., J.T. Bloking, and Y.-M. Chiang, *Electronically conductive phospho-olivines as lithium storage electrodes.* Nat Mater, 2002. **1**(2): p. 123-128.

36. Kang, B. and G. Ceder, *Battery materials for ultrafast charging and discharging.* Nature, 2009. **458**(7235): p. 190-193.

37. Park, O.K., et al., *Who will drive electric vehicles, olivine or spinel?* Energy & Environmental Science, 2011. **4**(5): p. 1621-1633.

38. Lee, H., et al., *SEI layer-forming additives for LiNi0.5Mn1.5O4/graphite 5 V Li-ion batteries.* Electrochemistry Communications, 2007. **9**(4): p. 801-806.

39. Xu, M., W. Li, and B.L. Lucht, *Effect of propane sultone on elevated temperature performance of anode and cathode materials in lithium-ion batteries.* Journal of Power Sources, 2009. **193**(2): p. 804-809.

40. Lu, Y.-C., et al., *Probing the Origin of Enhanced Stability of "AlPO4" Nanoparticle Coated LiCoO2 during Cycling to High Voltages: Combined XRD and XPS Studies.* Chemistry of Materials, 2009. **21**(19): p. 4408-4424.

# 초 록

리튬 이차 전지가 기존의 IT 기기 기반의 소형전지에서 대형 전지(e.g. 전기자동차, 에너지 저장 시스템)로의 패러다임이 이동됨에 따라 수명특성이 더욱더 중요시되고 있다. 수명 특성에 영향을 미치는 요소에는 양극, 음극 소재의 지속적인 리튬 충방전 가역성과 안정적인 전해질 및 분리막의 물리적 내구성 등의 4대 전지 구성 소재의 개별적 특성에서 기인하는 부분과 유기 전해액의 한정된 전기화학적 안정창으로 인하여 필연적으로 충방전시에 형성되는 산화 환원 반응으로 생성된 표면 피막의 안정성 등이 있다. 현재, 후자의 경우를 개선하기 위하여 표면 피막을 안정화하여 장기수명특성을 향상시키고자 다양한 첨가제가 연구되고 있다.

그러나, 새로 고안한 첨가제의 실제 효과를 확인하기 위해서는 장기 충방전을 거쳐 수명 특성의 개선을 확인한 후, AC 임피던스 법 등의 전기화학적 분석과 XPS 등의 분광학적인 분석법을 사용하여 실제 이 첨가제가 어떤 기작으로 성능 개선을 유발하는지에 대하여 이해하는 접근 방법을 가져가는 경우가 대다수이다. 다만, 과거의 방법들은 실제 새롭게 제시된 첨가제의 성능 평가에는 많은 시간과 비용이 소모되는 산업적 측면에서의 단점이 존재한다. 이런 문제점으로 인하여, 전해액에 새로 추가된 첨가제의 성능을 평가하기 위한 빠르고 경제성에서 우수한 새로운 툴이 필요한 실정이다.

본 연구에서는 LSTA(Linear sweep thermammetry)법을 통하여 기존의 방법보다 단기간에 수명특성을 예측하고 이 방법에 대한 검증을 하고자 하였다. LSTA 법이란 인가한 일정 전압에서 온도를 올려주며 작동전극에서 흐르는 전류를 측정하는 분석법이다. 본 연구에서는 작동 전극을 느린 전류속도로 피막을 형성시켜 준 이후에 LSTA 법으로 분석함으로써, 흐르는 전류량을 확인하여 수명 특성을 예측하려 하였다. LSTA에서 예상되는 피막의 파괴로 인한 전류량의 크기는 기존의 고온 충방전 중의 피막거동의 퇴화의 정도, 즉 피막의 상대적 안정성과 유사할 것이라 예상하였고, 이에 근거하여 더 쉽고 빠르게 수명특성을 볼 수 있다는 점을 제시하고 이를 검증하였다.

LSTA를 통해 수명특성을 예측할 수 있다는 점을 연구하고자 본 연구에서는 $LiNi_{0.5}Co_{0.2}Mn_{0.3}O_2$를 사용하였다. NCM 523은 $LiNiO_2$의 고용량, $LiMnO_2$의 경제성, $LiCoO_2$의 안정한 전기화학 특성의 장점들을 결합시킨 3성분계 물질이다. 더 나아가 샘플 간의 피막특성을 다르게 하기 위하여 사용한 첨가제로 각각 고전압 및 고온에서 좋지 않은 성능을 가진 VC(Vinylene Carbonate)와 좋은 성능을 가진 PS(Propane Sultone), 그리고 아무런 첨가제를 사용하지 않은 전해액을 사용하였다. 이를 통하여 실제 잘 알려진 첨가제의 성질을 LSTA가 잘 나타낼 수 있는가를 검증하려 하였다.

4.7V의 일정한 전압에서 측정한 LSTA 결과와 실제 피막 거동이 유사함을 검증하기 위하여 상온(25 $^0$C)와 고온(60 $^0$C)에 대한 분석을 실행하였다. LSTA

에서 보여지는 산화 전류량이 25°C에서는 세 샘플간에서 큰 차이가 발견되지 아니하였고, 수명특성의 경향성 또한 이와 일치함을 확인하였다. 미분용량곡선(differential capacity plot)을 통해 오십 번의 충방전 후에 과전압 증가량 또한 세 샘플간에 비슷함을 확인하였고, AC 임피던스 데이터 역시 필름 저항의 증가량이 세 샘플간에 비슷함을 나타내었고, 이를 통하여 LSTA데이터의 검증을 실행하였다. 다음 설정 온도인 60 $^{0}$C에서는 세 샘플간의 전류량 차이가 VC, bare, PS의 순서로 나타남을 확인하였고, 이 전류량에 따라 경향성을 가지면서 수명특성이 PS, bare, VC의 순서로 우수함을 확인하였다. 또한 이와 일치하는 경향성을 가지며 과전압 증가량이 차이남을 확인하였고, 임피던스에서 필름 저항의 증가량이 차이남을 확인하였다. 또한 XPS의 top-most의 lattice oxygen과 Ni의 intensity로부터 이 차이가 필름의 두께에서 기인함도 확인하였다. 이 결과로부터, LSTA법을 사용하여 실제 피막의 상대적 안정성을 비교할 수 있으며, 이를 통한 수명 특성 예측이 가능함을 검증하였다

주요어: 리튬 이차 전지, LSTA(Linear sweep thermammetry), 부동태 피막, 양극, 첨가제

학 번: 20012-22586